Atmos. Meas. Tech., 8, 1447–1466, 2015
www.atmos-meas-tech.net/8/1447/2015/
doi:10.5194/amt-8-1447-2015

Atmospheric Measurement Techniques
Open Access

Cross-validation of IASI/MetOp derived tropospheric δD with TES and ground-based FTIR observations

J.-L. Lacour[1], L. Clarisse[1], J. Worden[2], M. Schneider[3], S. Barthlott[3], F. Hase[3], C. Risi[4], C. Clerbaux[1,5], D. Hurtmans[1], and P.-F. Coheur[1]

[1]Spectroscopie de l'Atmosphère, Service de Chimie Quantique et Photophysique, Université Libre de Bruxelles, Brussels, Belgium
[2]Jet Propulsion Laboratory, California Institute of Technology, Pasadena, California, USA
[3]Institute for Meteorology and Climate Research (IMK-ASF), Karlsruhe Institute of Technology, Karlsruhe, Germany
[4]UPMC Univ. Paris 06, CNRS/INSU – UMR8539, LMD-IPSL, Paris, France
[5]UPMC Univ. Paris 06; Université Versailles St-Quentin, CNRS/INSU, LATMOS-IPSL, Paris, France

Correspondence to: J.-L. Lacour (jlacour@ulb.ac.be)

Received: 2 October 2014 – Published in Atmos. Meas. Tech. Discuss.: 12 November 2014
Revised: 18 February 2015 – Accepted: 26 February 2015 – Published: 20 March 2015

Abstract. The Infrared Atmospheric Sounding Interferometer (IASI) flying onboard MetOpA and MetOpB is able to capture fine isotopic variations of the HDO to H_2O ratio (δD) in the troposphere. Such observations at the high spatio-temporal resolution of the sounder are of great interest to improve our understanding of the mechanisms controlling humidity in the troposphere. In this study we aim to empirically assess the validity of our error estimation previously evaluated theoretically. To achieve this, we compare IASI δD retrieved profiles with other available profiles of δD, from the TES infrared sounder onboard AURA and from three ground-based FTIR stations produced within the MUSICA project: the NDACC (Network for the Detection of Atmospheric Composition Change) sites Kiruna and Izaña, and the TCCON site Karlsruhe, which in addition to near-infrared TCCON spectra also records mid-infrared spectra. We describe the achievable level of agreement between the different retrievals and show that these theoretical errors are in good agreement with empirical differences. The comparisons are made at different locations from tropical to Arctic latitudes, above sea and above land. Generally IASI and TES are similarly sensitive to δD in the free troposphere which allows one to compare their measurements directly. At tropical latitudes where IASI's sensitivity is lower than that of TES, we show that the agreement improves when taking into account the sensitivity of IASI in the TES retrieval. For the comparison IASI-FTIR only direct comparisons are performed because the sensitivity profiles of the two observing systems do not allow to take into account their differences of sensitivity. We identify a quasi negligible bias in the free troposphere (−3 ‰) between IASI retrieved δD with the TES, which are bias corrected, but important with the ground-based FTIR reaching −47 ‰. We also suggest that model-satellite observation comparisons could be optimized with IASI thanks to its high spatial and temporal sampling.

1 Introduction

Water vapour in the troposphere has a central role in the climate system (Pierrehumbert et al., 2007; Sherwood et al., 2010). Yet there are important uncertainties associated with the mechanisms controlling tropospheric water vapour distribution throughout the globe, leading to systematic biases in actual representations (Soden and Bretherton, 1994; Brogniez and Pierrehumbert, 2007; Allan et al., 2003; Bates and Jackson, 1997; Pierce et al., 2006) and an important spread in future climate predictions (Soden and Held, 2006; de Forster and Collins, 2004). In particular, the cloud feedback is responsible for most of the spread in the different climate models (Cess et al., 1990; Dufresne and Bony, 2008) because of the various representations of associated processes in the different models. Recently, Sherwood et al. (2014) showed that, among 43 climate models, the different ways of simulating

convective mixing between the lower and middle tropical troposphere was responsible for about half of the variance in climate sensitivity. It is thus crucial to improve representation of hydrological processes.

Observations of water vapour isotopologues have the potential to reveal information on the processes controlling humidity. The different water isotopologues are indeed characterized by distinct vapour pressures and are therefore sensitive to phase changes: the heavy isotopologues ($H_2{}^{18}O$, HDO) preferentially condense while the light ($H_2{}^{16}O$) preferentially evaporates. Hence, the heavy-to-light isotopologue ratio provides useful information on the air mass history and can be used to constrain hydrological processes (Strong et al., 2007; Worden et al., 2007; Samuels-Crow et al., 2014; Risi et al., 2012a, b; Noone, 2012). The ratio is commonly expressed in δ notation:

$$\delta\mathrm{D} = 1000\left(\frac{\frac{\mathrm{HDO}}{\mathrm{H_2O}}}{\mathrm{VSMOW}} - 1\right), \quad (1)$$

where VSMOW (Vienna Standard Mean Ocean Water) is the reference standard for water isotope ratios (Craig, 1961).

Among the different methods to determine the isotopic composition of water vapour, it has been shown that remote sensing instruments can be used to infer estimates of δD at a sufficient precision for scientific applications (Risi et al., 2012b), with the advantage that they provide measurements over regions and at altitudes that are not easily accessible. Space sounders also have the potential to provide global distributions (Worden et al., 2007; Frankenberg et al., 2009, 2013; Boesch et al., 2013). The Infrared Atmospheric Sounding Interferometer (IASI) (Clerbaux et al., 2009) onboard the MetOp meteorological satellite is particularly suited for measuring δD owing to its unique sampling characteristics (Schneider and Hase, 2011; Lacour et al., 2012). Indeed, IASI samples the atmosphere almost everywhere on the globe twice a day with a ground pixel size of 12 km at nadir.

Because of their inherent lack of vertical sensitivity, measurements derived from remote sounding instruments constitute a more or less complicated function of the quantity of the interest (Rodgers and Connor, 2003) and can not be regarded as true values. The regularization procedure used in the retrievals is in fact often such that they constitute the most probable estimate given the measurement and some a priori statistical information. Moreover retrieved quantities depend also on several parameters of the inversion such as the a priori, the spectroscopic line database, the spectral range etc. For all these reasons, the validity of quantities derived from remote sensing instruments always needs to be evaluated against other observations. It is at the same time crucial to document how different remote sensing products compare between them. In this paper we assess the validity of δD vertical profiles retrieved from IASI at ULB by comparing them with other available profiles of δD in the troposphere. We use the term "cross-validation" according to von Clarmann (2006) for this exercise as we compare IASI vertical profiles against profiles from other remote sounding instruments which do not constitute absolute values of the state of the atmosphere. Our study is similar to the recent cross-validation of IASI δD retrievals from KIT with ground-based FTIRs (Wiegele et al., 2014). We note that there has recently been an increasing number of absolute measurements of tropospheric δD (Schneider et al., 2014; Herman et al., 2014), which will be essential to validate δD profiles retrieved from the remote sounders and thus to ensure the optimal use of the latter, which are for now often limited to relative variations analyses (Risi et al., 2012b). In this study, although we do not use the absolute measurements, we perform the cross-validation with respect to instruments which have been evaluated against them. This allows us to infer some preliminary conclusions on how our retrievals would compare to these references.

For the cross-validation of IASI, we use δD profiles from the TES instrument onboard Aura (Worden et al., 2012) and from ground-based FTIRs from the MUSICA network (Schneider et al., 2012) which are both sensitive to δD in the same part of the troposphere as IASI. We do not perform the comparison with other space sounders, which provide δD retrievals in the upper troposphere or near the surface where IASI is generally less sensitive (Lacour et al., 2012; Schneider and Hase, 2011).

The main purpose of the cross-validation exercise presented here is to verify that two profiles from two different remote sounding instruments agree within their respective limitations (Rodgers and Connor, 2003), that is to say that the estimated profiles are well characterized by their error and sensitivity matrices. In Sect. 2 we introduce the methodology employed to adequately intercompare the different instrument products. Specifics of the δD retrievals (also referred to as $\mathrm{HDO}/\mathrm{H_2O}$ ratio retrieval) are also documented in this section. We then give a brief overview of the different instruments in Sect. 3. In Sects. 4 and 5 we detail the results of the comparison between IASI and TES and between IASI and the ground-based FTIRs, respectively.

2 Methodology to intercompare δD profiles

In this study we mainly follow the Rodgers and Connor (2003) methodology developed to intercompare indirect measurements. Its application to δD retrievals is described below.

2.1 Retrieval of the $\mathrm{HDO}/\mathrm{H_2O}$ ratio

Retrieving the $\mathrm{HDO}/\mathrm{H_2O}$ ratio at a sufficient quality from remote sounding instruments is challenging since the retrieval needs to be precise enough to capture the fine isotopic variations and sensitive over the large dynamical range

of water vapour concentrations in the troposphere. This requirement is antagonistic with the general formulation of the optimal estimation as the precision of the retrieval highly depends on the applied statistical constraint which itself limits the range of possible states. One way of overcoming this limitation is to introduce an inter-constraint between the two water isotopologues and to perform the retrieval on a logarithmic scale (Schneider et al., 2006; Worden et al., 2006). The different retrieval products we use here (Lacour et al., 2012; Worden et al., 2012; Schneider et al., 2012) have been obtained applying this constrained approach. One difficulty introduced by the constrained retrieval is the posterior characterization of the δD profiles as the averaging kernels and error covariance matrices obtained are indeed representative of the retrieved states log(H_2O) and log(HDO) and can not be directly applied to δD.

Schneider et al. (2012) have developed an elegant method to characterize the vertical profiles of H_2O and δD for retrievals which constrain the ratio log(HDO / H_2O). This method allows one to transform the products obtained in the {log(H_2O), log(HDO)} space into a proxy state {log(humidity), δD}. It is then possible to provide proxy error covariance matrices and averaging kernels for the δD profile which in turn facilitates its use for geophysical analyses.

In addition, the method allows for a minimization of the cross dependence of the H_2O retrieval on the δD retrieval and vice versa (Schneider et al., 2012). As retrieved H_2O and δD exhibit different vertical sensitivities (the sensitivity to δD being limited compared to H_2O) and are thus not fully representative of the same air mass, Schneider et al. (2012) recommend distinguishing two types of products. A product (type 1) for an optimal use of H_2O vertical profiles alone and a product (type 2) for consistent H_2O and δD data which are likely to be used together and need to be representative of the same air mass. This is achieved by reducing the H_2O profile to the δD retrieval sensitivity. In this paper we use this proxy state (type 2) to characterize δD profiles in terms of averaging kernels and error covariance matrices and all retrievals have therefore been a posteriori corrected to obtain a product of type 2. Specifically, according to Schneider et al. (2012) this is done by

$$\hat{\boldsymbol{x}}^* = \mathbf{P}^{-1}\mathbf{C}\mathbf{P}\left(\hat{\boldsymbol{x}} - \boldsymbol{x}_\mathrm{a}\right) + \boldsymbol{x}_\mathrm{a}, \tag{2}$$

with $\boldsymbol{x}_\mathrm{a}$ the a priori state vector, $\hat{\boldsymbol{x}}$ the estimated state vector {log(H_2O), log(HDO)} the profiles originally retrieved and $\hat{\boldsymbol{x}}^*$ the corrected state vector {log(H_2O), log(HDO)} that is used to compute the δD ratio of type 2. For the description of **P** and **C** matrices we refer to Schneider et al. (2012). These matrices ensure the reduction of vertical sensitivity and resolution of the H_2O profile as well as a correction of the cross dependence. Averaging kernels and error covariance matrices from the different retrievals have all been transformed into the {log(humidity), δD} proxy space.

2.2 Transformation between grids

A cross-validation exercise should compare like with like and consists of applying corrections to make the different retrievals comparable. A first step required for the cross-validation involves the adjustment of the different vertical grids on which the retrievals are performed. The state vectors, the error covariance matrices as well as the averaging kernel matrices need to be represented on the same grids to be comparable. The state vector and the error covariance matrices can be transformed into a coarser or a finer grid. Indeed, following Rodgers (2000) the state vector $\boldsymbol{x}$ on a fine grid is related to a reduce vector z on a coarser grid as

$$\boldsymbol{x} = \mathbf{W}z + \epsilon_W \boldsymbol{x} \tag{3}$$

with **W** the interpolation matrix and $\epsilon_W \boldsymbol{x}$ the error induced by the interpolation (Calisesi et al., 2005). The transformation of the state vector on a fine grid to a state vector on a coarser grid can be obtained via

$$z = \mathbf{W}^*\boldsymbol{x}, \tag{4}$$

where $\mathbf{W}^*$ is the pseudo inverse matrix of **W**. The error covariance matrix can be resampled on the coarser grid as follows:

$$\mathbf{S}_z = \mathbf{W}^*\mathbf{S}_x\mathbf{W}^{*T}. \tag{5}$$

For the averaging kernels, the interpolation is more complicated. For example, Calisesi et al. (2005) also use the linear transformation to resample the AVK on different grids as follows:

$$\mathbf{A}_z = \mathbf{W}^*\mathbf{A}_x\mathbf{W}. \tag{6}$$

The equation has been used to transform averaging kernels on different grids in the case of retrieved profiles from limb sounders (Ceccherini et al., 2003; Calisesi et al., 2005) which are characterized by high vertical resolution compared to nadir sounders. In our study, as can be seen in Fig. 1, the IASI grid is coarser than the one used for TES and FTIRs. We aim at representing the other retrievals on the same grid as IASI since extrapolation would lead to additional error. Applying Eq. (6) to TES averaging kernels led to satisfying interpolated averaging kernel matrices. In the case of the FTIR however, this could not be applied without a significant degradation of the matrix owing to the configuration of levels for the FTIR grid. To have the FTIR AVK on the IASI vertical grid we therefore interpolated the eigenvectors of the AVK. First, the FTIR averaging kernels matrix is decomposed into its eigenvectors (AVK $= \mathbf{V}\mathbf{D}\mathbf{V}^{-1}$); second, the leading eigenvectors are interpolated on the IASI grid ($\mathbf{V}' = \mathbf{W}\mathbf{V}$); and third, the FTIR averaging kernels are reconstructed with the interpolated eigenvectors but with the eigenvalues corresponding to the original AVK (AVK$' = \mathbf{V}'\mathbf{D}\mathbf{V}'^{-1}$). The AVK$'$ obtained is then used for the comparison.

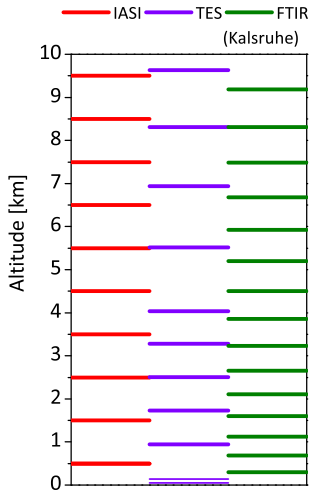

Figure 1. Retrieval grids of the different retrievals: IASI/ULB (red), TES averaged from retrievals above sea (purple), FTIR at Karlsruhe (green).

2.3 Expected difference between retrievals

The difference between two retrievals (now on the same grids) is given by Rodgers and Connor (2003) as

$$\delta = \hat{\boldsymbol{x}}_1 - \hat{\boldsymbol{x}}_2 = (\mathbf{A}_1 - \mathbf{A}_2)(\boldsymbol{x} - \boldsymbol{x}_c) + \epsilon_{x_1} - \epsilon_{x_2}, \quad (7)$$

with $\mathbf{A}_1$ and $\mathbf{A}_2$ the averaging kernel matrices of the two retrievals being compared, $\boldsymbol{x}$ the state vector and $\boldsymbol{x}_c$ the mean of the comparison ensemble. The latter, together with the covariance matrix $\mathbf{S}_c$, describe the ensemble of states over which the comparison is performed (Rodgers and Connor, 2003). We document how this ensemble is generated in the next subsection. The covariance of δ (Eq. 7) is given by

$$\mathbf{S}_\delta = (\mathbf{A}_1 - \mathbf{A}_2)^T \mathbf{S}_c (\mathbf{A}_1 - \mathbf{A}_2) + \mathbf{S}_{x_1} + \mathbf{S}_{x_2}, \quad (8)$$

with $\mathbf{S}_c$ the covariance matrix describing the comparison ensemble, and $\mathbf{S}_x$ the error covariance matrix due to observational error. Equation (8) evaluates the expected difference between two retrievals. The first term describes the contribution coming from the different vertical sensitivities of the two instruments and the two other terms, the respective contributions from the error covariances of each retrieval.

When the two retrievals to be compared exhibit very different vertical sensitivity profiles, the expected error can be very large. When it gets close to the expected natural variability of the quantity of interest, the comparison loses some significance. To deal with such situations one might reduce the effect of the smoothing error on the comparison by simulating one profile with the vertical sensitivity of the other. If the retrieval 2 is optimal with respect to the comparison ensemble and the retrieval 1 with less vertical sensitivity, the retrieved profile 2 can be smoothed with the averaging kernels of retrieval 1 to give

$$\hat{\boldsymbol{x}}_{12} = \boldsymbol{x}_c + \mathbf{A}_1 \left(\hat{\boldsymbol{x}}_2 - \boldsymbol{x}_c\right). \quad (9)$$

The averaging kernel matrix associated with $\hat{\boldsymbol{x}}_{12}$ is then $\mathbf{A}_1\mathbf{A}_2$. Equation (8) becomes

$$\mathbf{S}_{\delta_{12}} = (\mathbf{A}_1 - \mathbf{A}_1\mathbf{A}_2)\mathbf{S}_c(\mathbf{A}_1 - \mathbf{A}_1\mathbf{A}_2)^T + \mathbf{S}_{x_1} + \mathbf{A}_1\mathbf{S}_{x_2}\mathbf{A}_1^T.. \quad (10)$$

By doing so, the smoothing error will be smaller than in the direct comparison.

2.3.1 Correction for the use of different a priori

The different retrieved profiles of δD have been adjusted to take into account the use of different a priori by adding to each retrieved profile the term $(\mathbf{A} - \mathbf{I})$ $(\boldsymbol{x}_a - \boldsymbol{x}_c)$ (Rodgers and Connor, 2003) with $\boldsymbol{x}_c$ being the mean profile of the comparison ensemble which we defined as the a priori profile of TES for the IASI-TES comparison and as the FTIR a priori profile for the IASI-FTIR comparison.

2.3.2 Usefulness of the comparison and choice of the comparison ensemble

As said above, the comparison is useful if the difference between the two compared retrieved profiles is lower than the natural expected variability of δD. The latter is evaluated here by comparing covariance matrices with daily δD profiles from the isotope-enabled atmospheric model LMDZ (Risi et al., 2010). The model, nudged with ECMWF reanalysed winds, has demonstrated capabilities to reproduce reasonably well δD distributions throughout the globe (Risi et al., 2012b). We consider in our analysis the expected natural variability of δD at a quasi global scale (from 60° S to 60° N) but also at regional scales whenever relevant.

We also use the quasi global covariance matrix as the comparison ensemble covariance matrix $\mathbf{S}_c$ (Eqs. 10 and 8) which should describe the real ensemble of atmospheric possible states as well as possible (Rodgers and Connor, 2003).

2.4 Comparison of the δD–humidity relation

δD profiles alone do not provide information on hydrological processes. They become useful when analysed together with humidity variations as this combination will determine an enrichment or depletion of the air mass accompanying a humidifying or drying process. In a first approximation isotopic composition of water vapour follows a Rayleigh distillation curve (Rayleigh, 1902) which predicts a continuous depletion of the heavy isotopologue during condensation. This relation can be approximated to the following linear relation (Noone, 2012):

$$(\delta\mathrm{D} - \delta\mathrm{D}_0) \approx (\alpha - 1)\ln\frac{q}{q_0}, \quad (11)$$

with q the specific humidity, α the effective fractionation coefficient and the subscript 0 describing the initial conditions (isotopic composition and mixing ratio of the source depending on latitude and temperature).

Observations of δD and H_2O are especially interesting when they show deviations from Rayleigh distillation curves. For example, mixing of different air masses will give the resulting air mass an isotopic signature more enriched than a Rayleigh distillation for a same q (Noone et al., 2011; Galewsky et al., 2007). In contrast, re-evaporation of rain drops in convective environments enhances the depletion of the heavy isotopologue in water vapour (Worden et al., 2007; Risi et al., 2008), resulting in a more depleted isotopic signature. These simple examples are two extremes in the processes affecting isotopic composition. In general the isotopic composition is determined by a complex interplay between enriching and depleting processes.

Analysis of retrieved δD from remote sounders needs to be considered carefully as the retrieval of H_2O influences the retrieved values of δD. This is especially true in our case where a statistical constraint is added between HDO and H_2O. Even if the influence of H_2O retrieval on δD is minimized by applying the methodology of Schneider et al. (2012) it is important to verify that observations of δD together with humidity can actually show some deviations from Rayleigh curves. For example in their cross-validation and validation study, Schneider et al. (2014) and Wiegele et al. (2014) show that remote sensing products and in situ measurement exhibit similar anomalies in the δD–q space, demonstrating that the former are indeed sensitive to hydrological conditions. We also address this issue in the present paper by comparing the observations from the different instruments in the q–δD diagrams and by analysing the spatio-temporal variations of the q–δD relation.

3 Products overview

3.1 IASI

IASI is a Fourier transform spectrometer flying onboard the European meteorological polar-orbit MetOp satellite. It measures thermal infrared radiation emitted by the Earth and the atmosphere with a spectral resolution of $0.5\,cm^{-1}$ (apodized) and a low radiometric noise of 0.1–0.2 K (in the spectral range used for the retrieval) for a reference blackbody at 280 K (Hilton et al., 2012; Clerbaux et al., 2009). The sampling characteristics of the instrument (a measurement almost everywhere twice a day) result in about 1.2 million spectra per day. Currently there is no algorithm available which is capable of processing this volume of data for δD in near-real-time but there are two different retrieval schemes that have been developed to retrieve δD from IASI spectra for limited periods or regions: the one we are concerned with in this paper, developed at Université Libre de Bruxelles (ULB) with the radiative transfer code "Atmosphit" and the one developed at KIT within the MUSICA project, which applies the radiative transfer and retrieval code PROFFIT. Both retrieval schemes are optimized to constrain the log(HDO / H_2O) ratio but present significant differences. The main differences are the spectral range used and the strength of the statistical constraint used: at KIT, a wide range of the IASI spectra is used in the retrieval ($1190 \rightarrow 1400\,cm^{-1}$) with a strong statistical constraint while at ULB the retrieval uses a shorter spectral range ($1195 \rightarrow 1253\,cm^{-1}$) and a moderate statistical constraint. More details can be found in Lacour et al. (2012) for the ULB retrieval and in Schneider and Hase (2011) for the KIT retrieval. In what follows the IASI retrieval we refer to is the one developed at ULB. The retrieved profiles have been theoretically characterized and evaluated against model simulations in Lacour et al. (2012) for scenes above the oceans. It has been shown that the retrieved profiles were sufficiently sensitive and precise in the free troposphere with an error on the 3–6 km layer evaluated to 38 ‰ on a single measurement basis. In the present study, scenes above land and sea from tropical to Arctic latitudes are considered. Note that only measurements from MetOpA, the first of the series of MetOp satellites, are analysed.

3.2 TES

The TES instrument aboard the Aura satellite since 2004 (Beer et al., 2001) is, like IASI, a Fourier transform spectrometer measuring the thermal infrared radiation emitted by the Earth and the atmosphere. The spectral region covered by TES ranges from 650 to $3050\,cm^{-1}$. The spectral resolution of TES (apodized spectral resolution of $0.1\,cm^{-1}$) is higher than that of IASI ($0.5\,cm^{-1}$), while the instrumental noise is larger. The TES sampling (limb and nadir measurements) is characterized with 3 different observational modes (global survey, step-and-stare, transect) allowing for different spatial coverage. In global survey mode TES takes one nadir observation every 180 km approximately. We used TES V005 Lite data (Worden et al., 2012) which are bias corrected for a suspected problem in HDO spectroscopic parameters. The TES retrieval scheme uses a wide spectral range from 1190 to $1320\,cm^{-1}$. This version of TES data was recently validated with aircraft measurements above Alaska by Herman et al. (2014) and a remaining bias of +37 ‰ has been identified. Observations of δD from TES available at a global scale from September 2004 have already been widely used to study hydrological processes.

3.3 Ground-based FTIR

The project MUSICA (MUlti-platform remote Sensing of Isotopologues for investigating the Cycle of Atmospheric water) aims to provide tropospheric H_2O and δD data sets from different instruments (Schneider et al., 2012). It is subdivided in three components: (1) the ground-based remote sensing component (ground-based FTIR from NDACC network), (2) the space-based component (IASI-KIT) and (3) an in situ component with cavity ring-down measurements. Here we work with component (1) of MUSICA

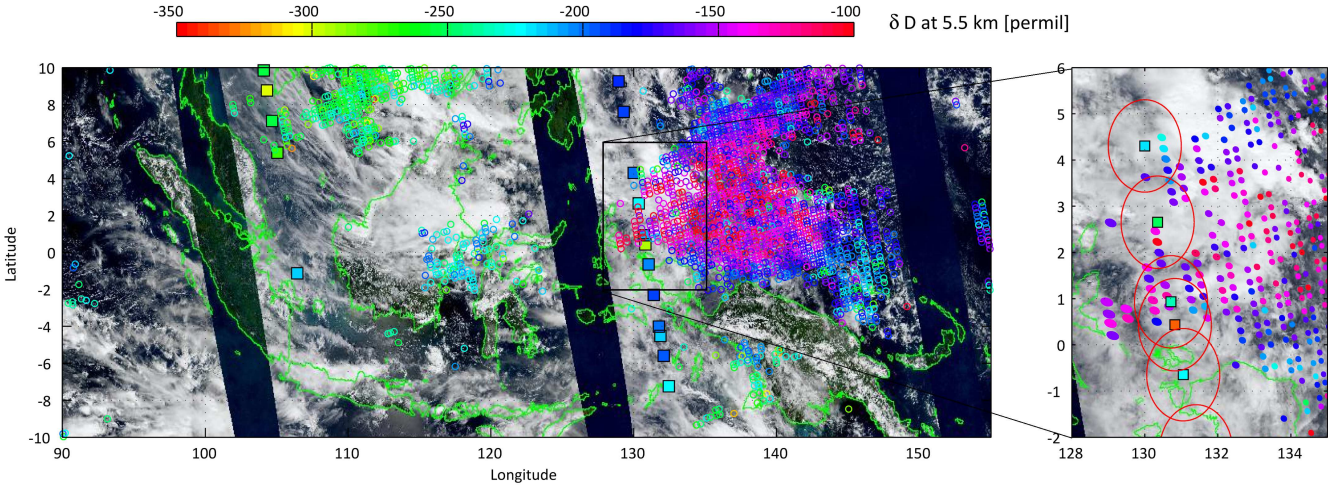

Figure 2. Illustration of the collocation between TES and IASI measurements for the IASI descending orbit (PM) on 18 January 2011 above the Pacific and Indian oceans. TES and IASI ground pixels are represented by square and ellipses respectively. The colour scale indicates the retrieved values of δD at 5.5 km. The background is a MODIS picture taken the same day. On the right panel, IASI pixels are represented at their real sizes.

and use ground-based FTIR measurement from 3 NDACC stations: Izaña (28.3° N, 16.5° W, 2367 m a.s.l.), Karlsruhe (49.1° N, 8.4° E, 111 m a.s.l.) and Kiruna (67.8° N, 20.4° E, 419 m a.s.l.). δD observations from these sites have been used previously for a comparison with IASI using the KIT retrieval scheme (Wiegele et al., 2014).

4 Comparison IASI vs. TES

4.1 Data sets description and collocation criterion

With its exceptional sampling characteristics, IASI provides a huge amount of data which requires important computing resources and appropriate algorithms to fully treat it (Hurtmans et al., 2012). For the retrieval of HDO / H_2O ratios these resources are, for the time being, limited and thus IASI δD availability is also limited. For this cross-validation two δD data sets are considered: (1) the full year 2010 along a meridional gradient in the Atlantic (from −60° S to 60° N and from 30 to 25° W) that we will refer to MD data set, (2) the period 2010–2012 above the Indian and Pacific oceans (15° S to 10° N and from 65 to 155° E) hereafter called the PIO data set. To illustrate the difference between TES and IASI sampling note that the PIO data set from March 2010 to December 2010 includes about 20 000 δD retrievals from TES and 4.5 million from IASI (cloud free measurements).

For each TES measurement, IASI measurement was selected if it was taken within a radius of 0.5° for the PIO data set and 1° for the MD data set as there was less data. Fig. 2 illustrates the spatial collocation of TES (squares) with IASI (ellipses) measurements for the descending orbit (PM) on 18 January 2011 above the maritime continent. Only IASI pixels that are within the red circles (right panel of Fig. 2) are considered for the comparison. It is not possible to have less than 4 h difference between the two instruments as this corresponds to the time delay between their day and night overpass times. The temporal collocation is such that we compare TES daytime measurement (13:30) only with IASI daytime measurement (09:30) and the same for the evening/night. In addition to these criteria, we also carried out a filtering on the air mass history based on backward trajectory analysis. For each TES measurement, backward trajectory was computed with HYSPLIT (Draxler and Hess, 1998). The data was rejected if the position of the air mass four hours before the TES measurement was too far (2.5°) from the IASI measurement. This 2.5° threshold has been defined by analysing the statistical differences between the TES and IASI integrated 3–6 km column and the distance of the air mass. We found that a spatial mismatch above 2.5° led indeed to significant differences.

Despite the strict collocation criterion used, some mismatches due to the natural variability of δD could arise. The spatial mismatch within circles of 0.5 to 1° is assumed to be inferior to the error on IASI retrieval and is thus unlikely to control the total difference expected between TES and IASI. For example, the 1σ standard deviation at 4.5 km on IASI retrieved profiles within cell of $1° \times 1°$ is about 22 ‰. In Wiegele et al. (2014), the authors estimated the error due to spatial mismatch for similar distances of about 18 ‰. The impact of a temporal mismatch is more difficult to estimate and might affect the total difference budget to some extent, especially above the maritime continent where convection has a pronounced diurnal cycle.

Comparison of one TES observation vs. several IASI observations

Generally, intercomparison studies are carried out by comparing one observation vs. another observation. Because the observational error on the IASI retrieval is relatively important (38 ‰ in the free troposphere; Lacour et al., 2012) compared to TES, to the FTIR and also compared to the expected natural variability of δD, the comparison between a couple of δD profiles could have limited utility. To cope with that, we chose to average all the IASI measurements fulfilling the collocation criteria with one TES δD observation. By doing so, the IASI observational error is lowered by the square root of N, the number of observations. Likewise, the error covariance matrix of the IASI error of Eqs. (8) and (10) is divided by N. Generally the number of IASI observations available around one TES observation ranges from 1 to 15.

4.2 Retrieval characteristics

Figure 3 shows typical averaging kernels for IASI and TES at tropical latitudes. These averaging kernels correspond to δD proxy averaging kernels (Schneider et al., 2012). For IASI, the resolution of the averaging kernels is quite coarse, about 4–5 km and the information of the retrieval comes mainly from the 0–3 and 3–7 km layers. The peaks of the averaging kernels are not perfectly located at their nominal altitude especially above 6 km indicating that the retrieved state above that altitude is mainly sensitive to variations of the real state at lower altitude. The degrees of freedom (DOFS) for this typical retrieved profiles of IASI is 1.7. Compared to IASI, TES averaging kernels show better resolved structures with a finer resolution and the averaging kernels all peak at their nominal height. The degree of freedom of 2.2 indicates two decorrelated levels of information, one in the lowest troposphere (0–3 km) and another in the free troposphere.

This situation is representative of tropical latitudes and indicates there a better sensitivity of TES to δD. The vertical sensitivity is however affected by local conditions such as humidity content, temperature profiles and surface temperature. Figure 4 shows the degrees of freedom for TES and IASI along the meridional gradient data set. One can see that the IASI DOFS present fewer variations than TES with latitude. More specifically, DOFS for IASI varies only between 1.5 and 2, while TES DOFS vary between high values (2–2.3) at tropical latitudes and lower values (0.5–2) at higher latitudes. The stability of the δD DOFS from IASI, as we explain in Appendix A, is due to a compensating effect of better sensitivity with increasing surface temperature but lower sensitivity with increasing humidity. Yet the higher sensitivity of IASI over TES at high latitude remains surprising and requires further investigations.

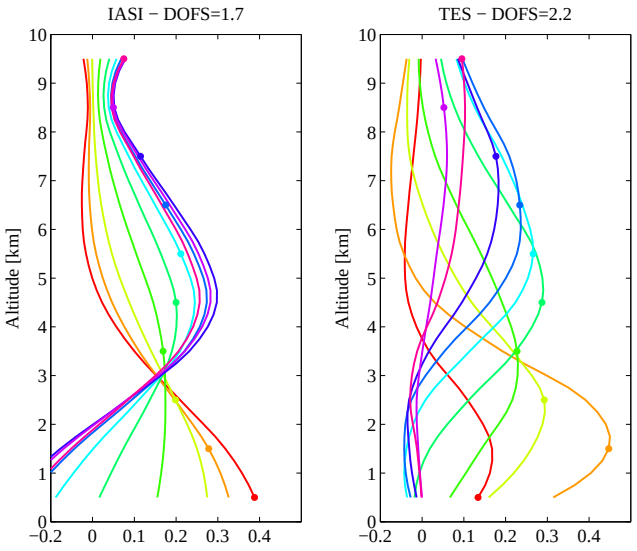

Figure 3. Typical averaging kernels in {δD} proxy space for IASI (left panel) and for TES (right panel) for a tropical scene (2.5° N). The nominal heights of the kernels are marked by filled circles.

4.3 Expected difference

For this comparison the retrievals of IASI and TES have been (1) a posteriori corrected for the cross-correlation interferences between H_2O and δD, (2) TES data have been re-gridded on the IASI grid and (3) corrected for the use of different a priori. To compute the expected agreement we use the quasi global $\mathbf{S}_c$ computed from the LMDZ model. Note that IASI and TES retrievals are not optimal with regard to the comparison ensemble defined by $\mathbf{S}_c$ since they each use different a priori covariance matrices. The $\mathbf{S}_c$ is more loose than the one ($\mathbf{S}_a$) used in TES retrievals and more constrained than the one used in IASI retrievals. The same $\mathbf{S}_c$ is used for the entire intercomparison.

Figure 5 shows for the retrievals above the PIO data set the total expected difference (black curve) from the comparison IASI vs. TES and its different contributions from the observational and smoothing error. For the PIO data set TES retrievals have more sensitivity to δD, we thus smoothed TES retrieved profiles with IASI averaging kernels for a more like-with-like comparison.

The direct comparison (no smoothing) is shown on the left panel of Fig. 5 and the smoothed comparison on the right panel. The total expected difference (black curve) of the direct comparison ranges from 120 ‰ at the lowest layer to 55 ‰ at 4.5 km, increasing again up to 68 ‰ at 7.5 km. The total expected difference is largely controlled by IASI observational error in the 0–2 km layer and above 6 km. In the free troposphere the difference of vertical sensitivities (smoothing error) between the two sounders also has an impact on the direct comparison. Note that IASI's observational error exceeds the δD global variability above 7 km and at 0.5 km,

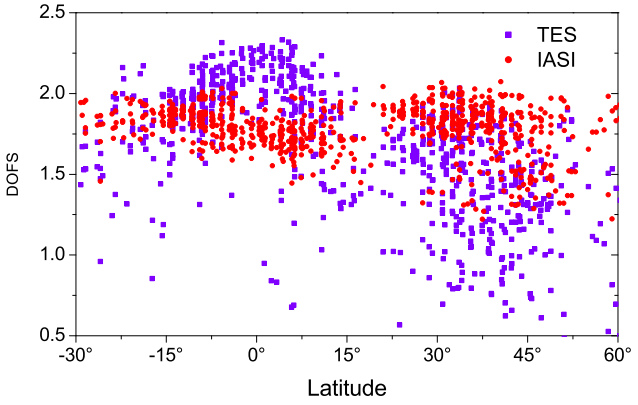

Figure 4. TES (purple) and IASI (red) degrees of freedom for δD along the meridional gradient.

and this is because the a priori covariance matrix ($\mathbf{S}_a$) used in the IASI retrieval is larger than the $\mathbf{S}_c$ used for the comparison. This error budget indicates that the direct comparison is relevant in the free troposphere when it refers to the expected natural variability of δD at global scale (dark blue bold line). However at a more regional scale (here the tropical variability given by the light blue bold line) the direct comparison is less significant since the total expected difference (55 ‰) is very close to the expected natural variability of δD ($\sim$ 70 ‰).

The right panel of Fig. 5 shows a similar error budget but accounting for the difference in sensitivity between instruments. One can see that the smoothing contribution is significantly reduced compared to the direct comparison. TES observational error is also reduced mainly because the fine structures have been removed by the IASI averaging kernels. This does not, however, affect the total expected difference since this error was already relatively small. The total expected difference is now only controlled by IASI's observational error and is reduced to 38 ‰ at 3.5 km.

4.4 Expected vs. real differences

In the previous section we have described the differences expected from the comparison between TES and IASI based on the theoretical error budgets of the different retrievals. In this section we compare the theoretical error budget with the real differences between TES and IASI δD retrieved profiles. Those are taken as the SD of the difference TES-IASI in the δD profiles and are plotted as a green line in Fig. 5. For the direct comparison, we find that the real difference is lower than the expected one below 7 km. This indicates that the difference TES-IASI at these altitudes is in agreement with the theoretical error budget. The fact that the real difference exceeds the expected one above 7 km could be due to an underestimation of the IASI's observational error (since all other contributions are mostly negligible). When smoothing TES retrieved profiles with IASI averaging kernels the real differences decrease in the free troposphere where the smoothing

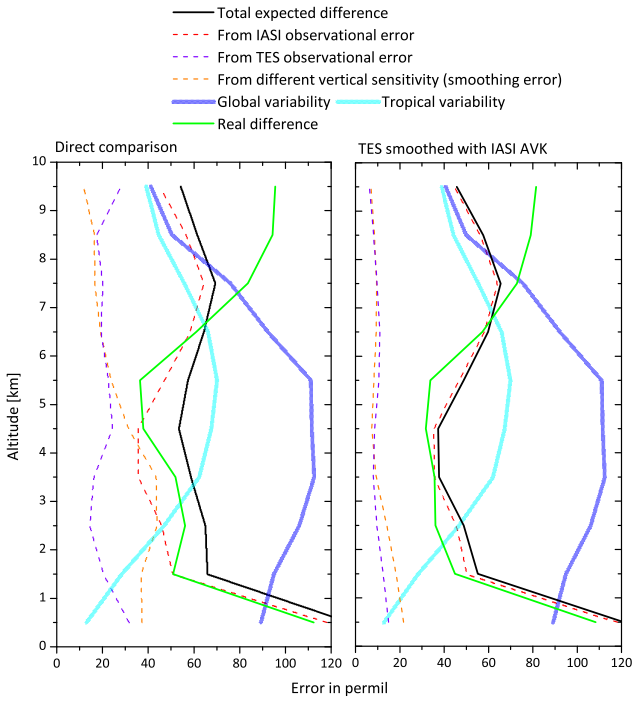

Figure 5. Expected difference of the IASI and TES retrieval at tropical latitudes and its different contribution sources according to Eq. (8) for the direct comparison (left panel) and to Eq. (10) for the smoothed comparison (right panel). The square root of the diagonal elements of the $\mathbf{S}_\delta$ matrix as well as the different contribution matrices are plotted. Real differences are also shown in green.

error was important. As for the non-smoothed comparison, the real difference remains below the theoretical one over the entire 0–7 km range.

While these figures are indicative of the error budget above the Indian and Pacific oceans, the variations in sensitivity are such that the budget will depend on humidity and temperature conditions. However, we found that the results presented in Fig. 5 are generally representative of all observations above the oceans. In the following subsection we provide a more statistical view on the agreement between TES and IASI.

4.4.1 Statistics of the agreement between IASI and TES

In this subsection we compare IASI to TES statistically for the MD and PIO data sets. We focus on retrieved δD values at 4.5 km which is the altitude where IASI is the most sensitive above the oceans. For the PIO data set we document the agreement for both the direct and the smoothed comparisons. For the MD data set we only consider the direct comparison because the sensitivity of TES – depending on the latitude (Fig. 4) – is sometimes higher and sometimes lower than IASI sensitivity. As we discussed in Sect. 4.2 the direct comparison is meaningful since the expected differences are substantially smaller than the natural variability at a global

Table 1. Comparison between IASI and TES δD at different heights for the PIO and MD data sets. σ(diff) is the SD of the difference between TES and IASI, in ‰. r is the Pearson correlation coefficient and m is the slope of the major axis regression TES vs. IASI (a value of m greater than one indicates that TES variability is greater than IASI variability). Direct comparison* is for the comparison restricted to the TES and IASI data having similar sensitivities (see text for details).

Data set	Altitude [km]	m		r		σ(diff) [‰]	
		Direct	Smoothed	Direct	Smoothed	Direct	Smoothed
PIO	0.5	0.09	6.24	0.13	0.30	91	72
	2.5	0.93	1.73	0.41	0.44	44	34
	3.5	1.18	1.12	0.50	0.55	41	30
	4.5	1.21	0.81	0.55	0.61	43	35
	5.5	1.27	0.79	0.57	0.39	42	41
	8.5	0.22	4.27	0.25	0.25	66	50
		Direct	Direct*	Direct	Direct*	Direct	Direct*
MD	0.5	0.38	0.37	0.28	0.27	71	72
	2.5	0.80	0.93	0.60	0.61	56	54
	3.5	0.98	1.18	0.67	0.73	49	35
	4.5	0.95	1.02	0.62	0.76	46	37
	5.5	1.04	1.12	0.47	0.59	68	50
	8.5	0.16	0.16	0.29	0.40	84	72

scale. We summarize the results from the comparison between IASI and TES in Table 1, in terms of 1σ SD, slope of the major axis regression (m) and Pearson correlation coefficient (r).

For the PIO data set we found a SD of the difference of 43 ‰ for the direct comparison which decreases to 35 ‰ when TES retrievals are smoothed with IASI averaging kernels. These values are in line with the theoretical estimations of the error. The correlation coefficients have values of 0.55 and 0.61 for the direct and smoothed comparison respectively. These values for the correlation are driven by the low signal-to-noise ratio of the compared quantities. Indeed, we calculated that we would expect a correlation coefficient no larger than 0.7 if we were to compare TES retrieved profiles with the same profiles perturbed by a random noise of 35 ‰. The correlation coefficient found for the IASI-TES comparison is coherent with this and demonstrates that TES and IASI δD co-vary well together. The slopes of the regression curves indicate that the TES variability is higher than the IASI one before the smoothing, but lower when the smoothing is taken into account.

For the MG data set, we only report statistics of the direct comparison but we distinguish a case with all collocated measurements and another (column "Direct" in Table 1) with only the collocated retrievals which have similar degrees of freedom ($\mathrm{DOFS_{IASI}} = \mathrm{DOFS_{TES}} \pm 0.3$). When all the measurements are taken into account we find at 4.5 km a SD of 46 ‰ in agreement with the theoretical error estimate. The correlation coefficient of 0.67 for this data set is significantly higher than for the PIO data set due to the larger amplitude of variations of δD along the meridional gradient (higher signal-to-noise ratio). The SD of the differences and the correlation coefficient are improved to 37 ‰ and 0.76 when only considering retrievals with similar degrees of freedom.

4.4.2 Systematic difference between IASI and TES

We calculate the mean bias for the 3–6 km layer as the mean difference between IASI and TES. We find a bias of +20 ‰ when using the non-smoothed data from PIO and MD data sets together and a bias of −3 ‰ when TES retrievals are smoothed with IASI averaging kernels (considering only collocated measurements where TES sensitivity is higher than IASI). The significant bias found for the non-smoothed data is probably due to the low vertical resolution of IASI. The averaging kernels indicate indeed that IASI is sensitive to a thicker layer of the atmosphere than TES which is likely to give a more enriched signal because of the mixing with information from the lowest layers. The bias when TES is smoothed according to IASI sensitivity is almost negligible. Although this may appear an encouraging result it is also questionable as TES data V005 are bias corrected, for uncertainties in spectroscopic line strength (Herman et al., 2014; Worden et al., 2011). As we use the same spectroscopic parameters for IASI retrieval, the high level of agreement could suggest another origin than spectroscopy for the bias applied to TES δD.

An accurate estimation of the bias on δD retrieved profiles from IASI would require further investigations including direct comparisons with available in situ profiles of δD in the troposphere (Schneider et al., 2014; Herman et al., 2014). Here, the purpose is to qualitatively document the bias between the different δD products.

4.5 Spatio-temporal variations of the δD–log(q) relation

For the MD data set we analyse δD–q relations at 4.5 km from each instrument for bins of 10°, in terms of the correlation coefficient between δD and log(q) and the slope of the regression curve δD vs. log(q). The variations of these parameters along the meridional gradient are shown in Fig. 6. The two instruments present very coherent variations of the δD–q relation. We also see that for each instrument the correlation coefficient δD–q varies strongly with latitude. In the case of a perfect Rayleigh distillation, δD would have a correlation coefficient of 1 with log(q) (Eq. 11). The values found for TES and IASI are the closest to 1 at 5° S and significantly lower at other latitudes, indicating that processes different than Rayleigh distillation are at play.

With the PIO data set we investigate both spatial and temporal variations of the δD–q relation at 3.5 and 5.5 km. We distinguish 3 different areas each of 30° longitudes (from west to east: A, B and C) in the entire data set and we also separate winter (DJF) from summer (JJA). The collocated pairs corresponding to these categories are plotted in Fig. 7. In this case, TES profiles (H_2O and δD) have been smoothed with IASI averaging kernels. We also plot the Rayleigh distillation curve (purple line) according to Eq. (11) with $q_0 = 3 \times 10^{-2}$ mol mol^{-1} and $\delta D_0 = -70$ ‰ which determine a lower limit for Rayleigh processes occurring at these latitudes. Above this curve, Rayleigh processes for drier source term and mixing processes can explain the isotopic composition. Below, only depleting processes can be at the origin of the observed values.

At 5.5 km, the seasonal and longitudinal patterns observed by TES and IASI are very similar. In particular one can see that for zone A the difference between the high δD values in summer and low values in winter are very different than what is observed in zone B with a majority of points below the Rayleigh distillation curve in DJF. In zone C, both instruments show a clear amount effect (enhancement of the depletion with high water vapour content) although IASI H_2O values seem slightly drier than TES.

At 3.5 km the seasonal and longitudinal variations are coherent between the two instruments, but the general agreement is less good than at 5.5 km. For example, an amount effect is well observed for each zone for TES while it can only be clearly seen in IASI retrievals in zone C. The reason of these differences is probably due to the better sensitivity of TES at these altitudes and below.

4.6 Comparison instrument–model

One of the specific applications of satellite measurements of δD is to evaluate performances of isotope-enabled GCM. TES observations have for example previously been used to evaluate GCM at a global scale (Yoshimura et al., 2011; Risi et al., 2012b) while IASI observations have been compared

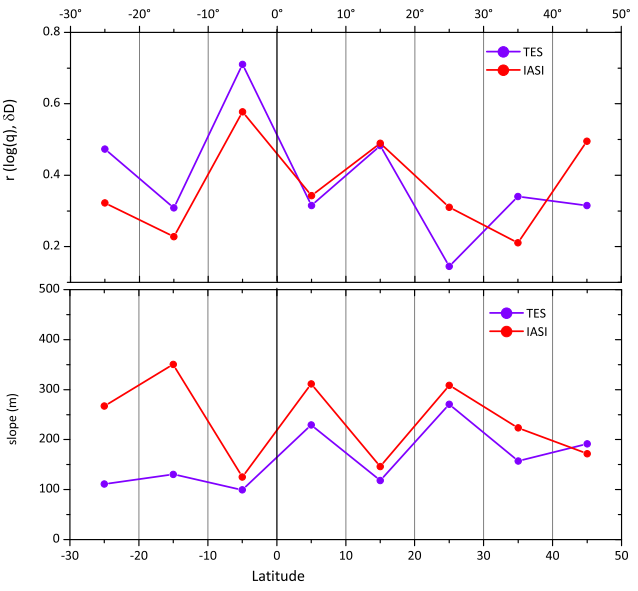

Figure 6. Top panel: variation of the correlation coefficient between log(q) and δD at 4.5 km along the meridional gradient for TES (purple) and IASI (red). Bottom panel: variation of the slope of the linear regression between log(q) and δD (spatial and temporal variability within the 10° bin) along the meridional gradient for TES (purple) and IASI (red).

to LMDZ at regional scales (Lacour et al., 2012; Pommier et al., 2014). Moreover, because of the integrated nature of the isotopologues ratio, models are often useful for interpreting the measurements. We take the opportunity of this cross-validation study to briefly investigate the differences that can arise from the comparison of a GCM with TES or with IASI. The goal here is twofold: (1) document how the instruments will differ in instrument–model comparisons and (2) illustrate the impact of IASI sampling in model–observation comparisons.

We use the GCM LMDZ (Risi et al., 2010) that we consider as the reality. We also consider retrieved profiles from IASI and TES as the reality. The model outputs are thus not smoothed with any instrument vertical sensitivity. This is not an usual approach but it allows one to have an idea of how close observations are from reality. Indeed by not taking the instrument sensitivity into account during the comparison, retrievals are considered as an estimate of the true state with an error contribution due to the smoothing, rather than estimate of a state smoothed by the averaging kernels (which is done when smoothing model outputs with averaging kernels) (Rodgers, 2000). We use the Pearson correlation coefficient as a metric of the agreement between LMDZ and the retrieved δD between 3 and 6 km, and the results are reported in Table 2. We have subdivided the MD data set in 2 different latitudinal groups according to the TES sensitivity: tropical observations located between 15° S and 15° N and subtropical to mid-latitude observations located between 15 and 45°

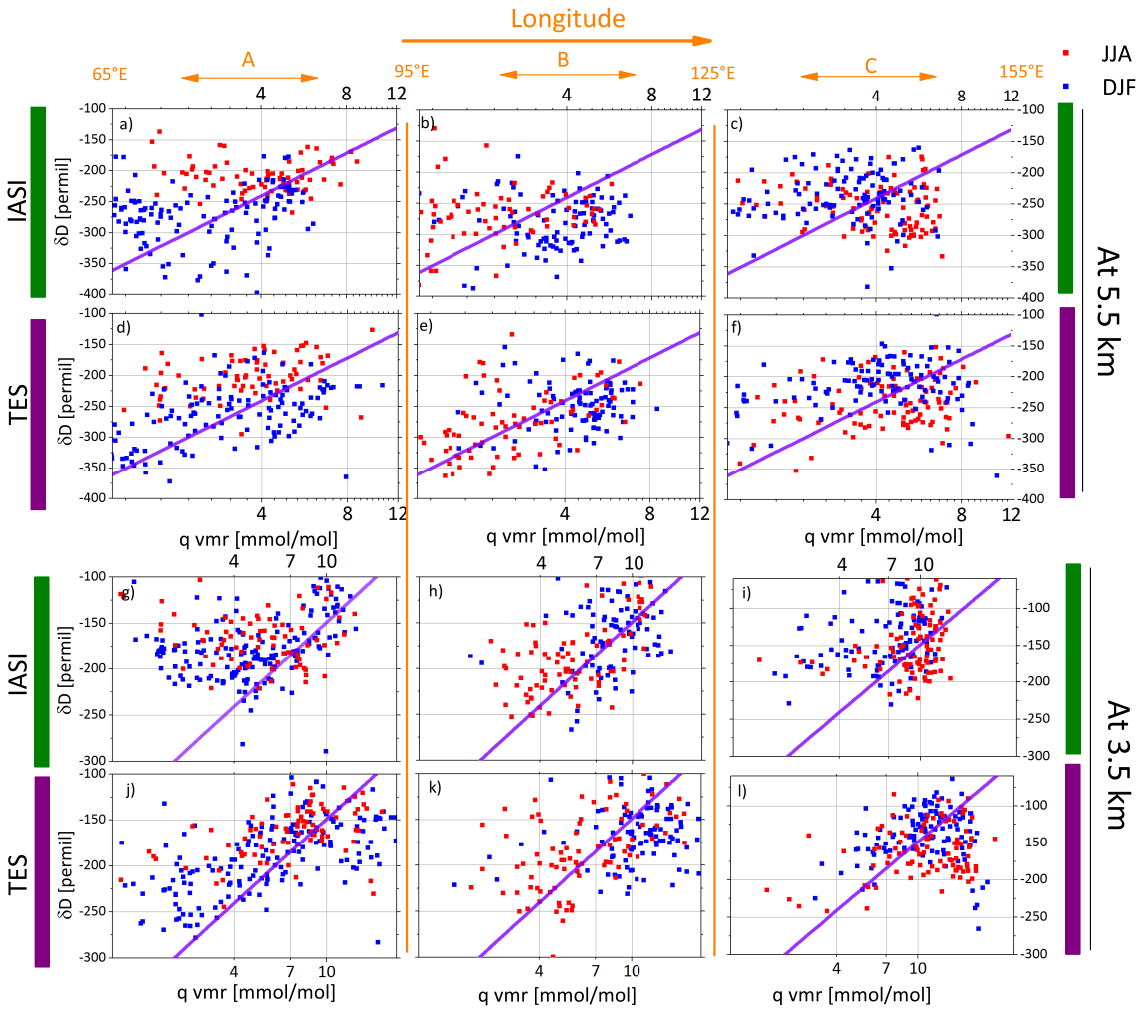

Figure 7. Spatio-temporal variations of the δD–q relation for the PIO data set. Retrieved δD and q are separated in three longitudinal boxes of 30° (A, B, C) from 65 to 155° E to highlight spatial variations. Winter (DJF, blue squares) and summer (JJA, red squares) are also separated to highlight seasonal variations. **(a–c)** correspond to IASI retrieved values at 5.5 km, and **(g–i)** to IASI retrieved values at 3.5 km. **(d–f)** correspond to TES retrieved values at 5.5 km, and **(j–l)** to TES retrieved values at 3.5 km. The purple line represents a Rayleigh distillation curve computed according to Eq. (11) with $q_0 = 0.03\,\mathrm{mol\,mol^{-1}}$ and $\delta\mathrm{D}_0 = -70\,‰$.

in both hemispheres. Note also that the comparison TES-LMDZ considers one TES observation vs. one LMDZ cell, and that this results in a worse agreement than previous studies that generally average TES observations over time and/or space.

For the PIO data set the values found in Table 2 show that the comparison LMDZ vs. TES shows a better correlation coefficient (0.26) than for the LMDZ vs. IASI comparison (0.15). This is also true for the MD data set at tropical latitudes with a slightly higher correlation coefficient of 0.46 and 0.30 for TES and IASI respectively. In contrast, for the subtropical to mid-latitude observations, we find a better correlation coefficient for the LMDZ vs. IASI comparison (0.42) compared to the LMDZ vs. TES comparison (0.30). The better agreement between LMDZ (reality) and IASI above 15° makes sense since we observe a significant decrease in TES sensitivity at these latitudes (see Fig. 4).

With the PIO data set we investigate how the number of available observations can impact a model–instrument comparison. This is interesting because the number of daily IASI observations in one model cell (3.75° × 2.53°) on a given day can be very large. Indeed, from the histogram in Fig. 8 we see that there is about 25 % of the LMDZ cells that contains 1 to 10 observations and about 12 % that contains 90 observations or more. The average number of observations available per cell is 46. The correlation coefficient between IASI and LMDZ increases compared to a one-to-one comparison, due on one hand to the decrease of the observational error by $\sqrt{(N)}$ when averaging several observations, and on the other hand to the better sampling of the model cell by IASI that allows to capture the variability of δD within this cell.

Table 2. Pearson correlation coefficients between LMDZ and TES/IASI for the PIO and MD data sets at 4.5 km.

	Orbit	Comparison	r	N
Pacific and Indian oceans	Day	TES vs. LMDZ	0.26	5636
		IASI vs. LMDZ	0.15	5636
	Night	TES vs. LMDZ	0.25	5636
		IASI vs. LMDZ	0.16	5 636
Meridional gradient	Tropics: 15° S–15° N	TES vs. LMDZ	0.46	556
		IASI vs. LMDZ	0.30	556
	Subtropics to mid-latitudes: 15–45°	TES vs. LMDZ	0.30	591
		IASI vs. LMDZ	0.42	591

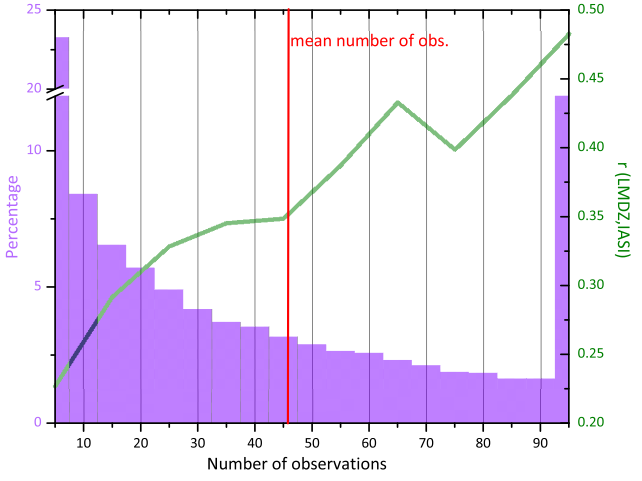

Figure 8. On the background (purple): histogram in percent of the number of IASI observations available per model cell for the LMDZ-IASI comparison (daily values) above the Pacific and Indian oceans data set. In green, the correlation coefficient between δD simulated by LMDZ and averaged δD from all observations available in the cell in function of the number of observations available.

When including less than 10 observations the correlation coefficient is below 0.25 but it increases up to 0.5 when including more than 90 observations. This is important and suggests that model–observation comparison could be largely improved by exploiting the unprecedented sampling of IASI.

To conclude this section we show in Fig. 9 how the two instruments map δD and H_2O variations above the Pacific and Indian oceans. Since TES sampling is relatively sparse, collocated retrieved values of δ at 5.5 km are averaged on three-month periods on cells of $2.5° \times 2.5°$. In that figure, TES retrieved values are not smoothed with IASI averaging kernels in order to ensure that TES retrieved profiles are not degraded to a lower sensitivity. δ variations are represented in relative values with respect to the mean of the data set to avoid the impact of the bias on the comparison. One can see on Fig. 9 that seasonal distributions of δ (panels a and b) are very similar for both instruments with the spatial structures of enriched and depleted zones being quasi identical. The same comparison with water vapour shows that humid and dry structures are also very similar in the TES and IASI retrievals and that the spatial structures of δ and H_2O exhibit very different patterns.

5 Comparison IASI vs. FTIR

5.1 Data sets description and collocation criterion

Three ground-based NDACC-FTIRs of the MUSICA network have been selected at different latitudes: Kiruna, Karlsruhe and Izaña. We consider FTIR and IASI observations collocated when there are no more than three hours between the two measurements and when the IASI observation is located in a radius of 1.5° around the measurement sites. We have applied the same approach as that for the IASI-TES comparison to make the comparison the most significant possible and when several IASI observations fulfilled the collocation criteria, we have averaged them to reduce the observational error. FTIRs and IASI δD profiles correspond to the years 2010, 2011 and 2012.

5.2 Retrieval characteristics

Representative averaging kernels for the three ground-based FTIR are plotted in Fig. 10 in comparison with the corresponding IASI averaging kernels. The IASI averaging kernels exhibit similar sensitivity profiles from high latitude to subtropical latitudes with degrees of freedom of 1.7, 1.9 and 1.7 at Kiruna, Karlsruhe and Izaña, respectively. As discussed before, the IASI retrieval sensitivity to δD comes from the free troposphere and also from the lowest layers of the atmosphere. At Arctic latitude (Kiruna) the IASI sensitivity close to the surface is the highest, probably owing to a favourable thermal contrast (Pommier et al., 2014). The FTIR averaging kernels exhibit similar sensitivity than IASI in terms of information content with DOFS of 1.5, 1.2 and 1.7 for Kiruna, Karlsruhe and Izaña respectively. The profiles of vertical sensitivities however significantly differ: Kiruna and Karlsruhe FTIR are mainly sensitive in the first

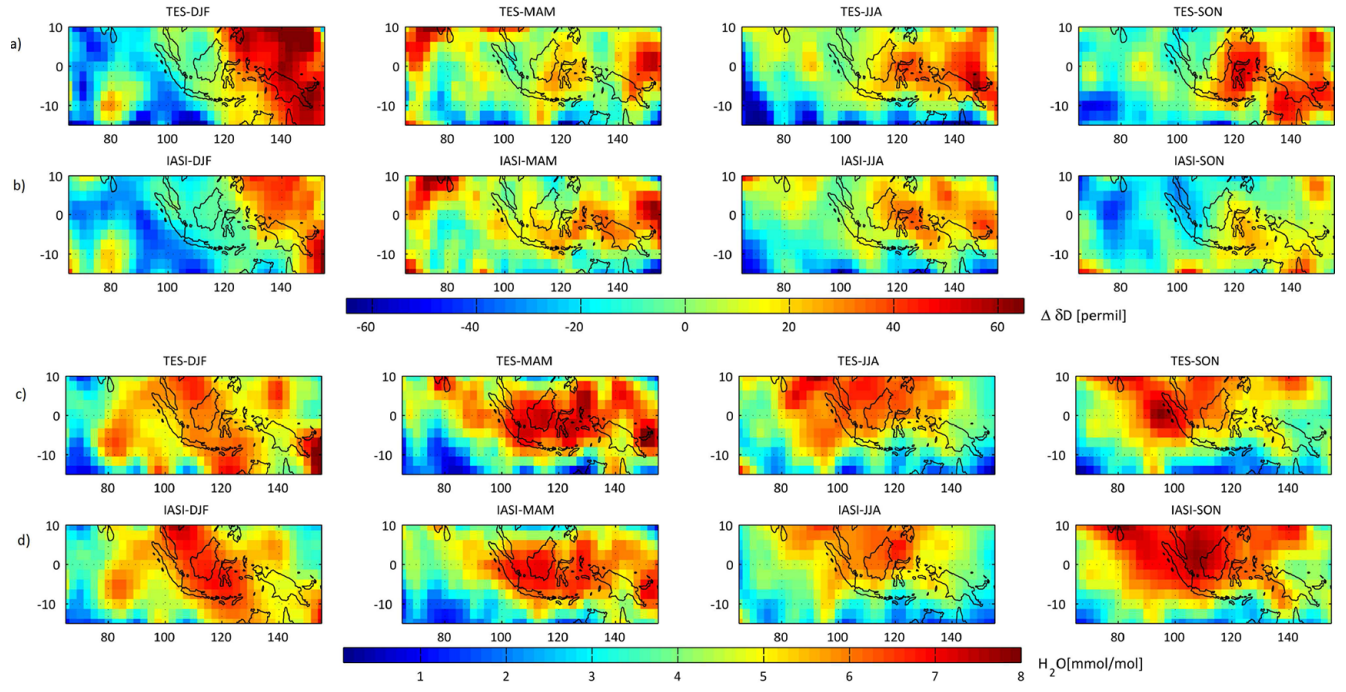

Figure 9. Seasonal distributions of δD and H_2O for the PIO data set at 5.5 km (2010) as seen by TES **(a, c)** and by IASI **(b, d)**. Only collocated pairs are used to compute the seasonal averages. The values are relative differences with respect to the mean of each data set.

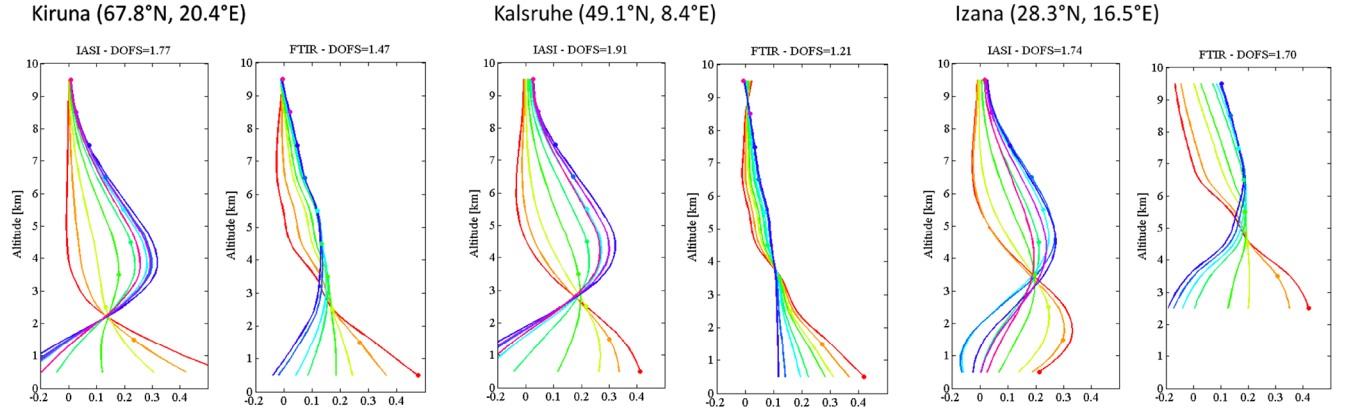

Figure 10. Averaging kernels in {δD} proxy space for the three different sites of the comparison: **(a)** and **(b)** for Kiruna, **(c)** and **(d)** for Karlsruhe and **(e)** and **(f)** for Izaña. **(a)**, **(c)** and **(e)** corresponding to IASI and **(b)**, **(d)** and **(f)** to the ground-based FTIR.

layers of the atmosphere and at Izaña, the FTIR exhibits sensitivity in the 3–5 km layer and also above 6 km.

5.3 Expected difference

The expected differences for the direct IASI-FTIR comparison are calculated according to Eq. (8) in the same way as for TES comparisons. The same $\mathbf{S}_c$ covariance matrix was also used. To evaluate the significance of the cross-validation, we compare the expected differences (black curve) in Fig. 11 at the three sites with the global δD variability (dark blue curve) but also with the regional variabilities (respectively green, brown and cyan curves for Kiruna, Karlsruhe and Izaña). The variabilities were calculated from LMDZ model profiles within a given 20° latitudinal band. We can see from Fig. 11 that Kiruna and Karlsruhe present very similar error budgets mainly controlled by IASI observational error while at Izaña the smoothing error also impacts the expected difference. For this comparison, we found that the smoothing of one instrument averaging kernels with the other was not productive. The comparison can thus not be optimized to take into account the different vertical sensitivities of the two instruments and only the direct comparison is discussed next.

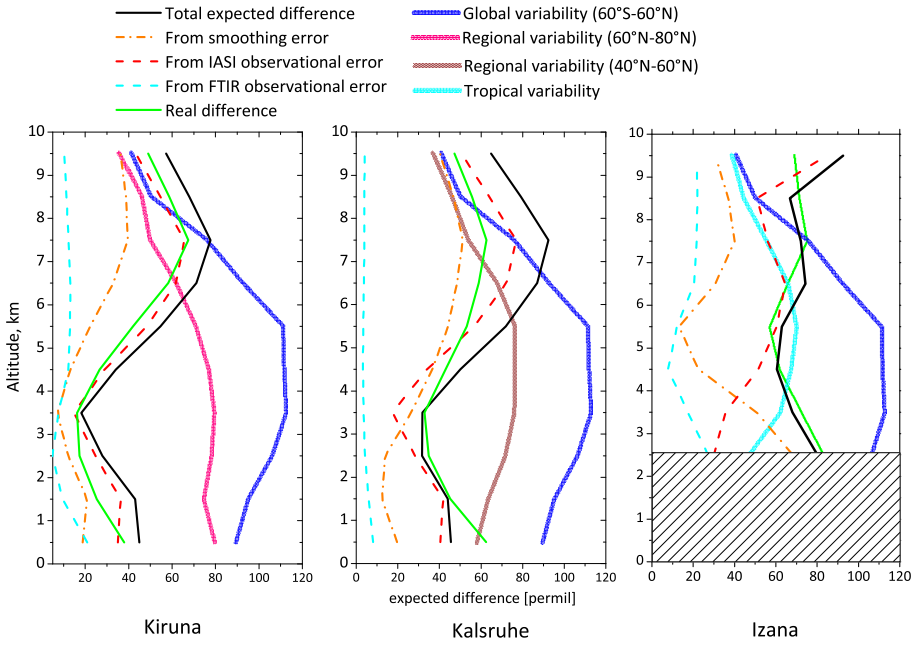

Figure 11. Same as Fig. 5 but for the comparison between IASI and the ground-based FTIR of Kiruna (left panels) and Karlsruhe (right panels).

The error difference budgets are shown in Fig. 11, representative of an average of the error budgets of a one month period. We note from Fig. 11 that the observational errors from the FTIR and from IASI are very different. For both sites the FTIR observational error is indeed lower than 20 ‰ throughout the vertical profile while IASI observational error ranges from 20 ‰ around 3–4 km to 80 ‰ in the upper troposphere. It is interesting here that the IASI observational error is significantly smaller in the lower troposphere compared to the error budget discussed previously in Fig. 5. This is mainly due to the fact that the two sites are on the continent, where the sensitivity of IASI to near surface δD is better due to more favourable thermal contrast. It is also interesting to note that the IASI observational error in the lower troposphere does not exceed the δD variability at a global scale and at a regional scale. This indicates that IASI retrievals provide relevant δD measurements in these conditions even in the boundary layer.

For Kiruna and Karlsruhe, the total expected difference is lowest in the free troposphere (about 20 ‰ for Kiruna and 35 ‰ for Karlsruhe) and highest in the upper troposphere. Compared to the regional expected variability of δD, the comparison might be considered useful below 5 km since both budgets show expected difference lower than the δD variability at regional level.

At Izaña, the total expected difference ranges from 90 ‰ at 2.5 km to about 60 ‰ at 4.5 km. At higher altitude the total expected error exceeds the natural variability of δD. In this case it is not only the IASI observational error that dominates the total difference expected. From 2.5 to 4 km the smoothing error is indeed large and contributes with both IASI and FTIR observational error. From 4 to 6 km the FTIR observational error becomes less important while at higher altitude it is the IASI observational error that becomes predominant again. The comparison appears significant with respect to the variability of δD at a global scale but not regional scale.

5.4 Expected vs. real differences

The real difference between the two instruments is calculated as the SD of the difference for each level for the corresponding time period of the computed error budgets. As in the IASI vs. TES comparison the SD profiles are plotted (green curves) on the error budget in Fig. 11 for the three sites.

We find that the SD profiles of the difference follow well the error profiles expected from the theoretical error (although with small deviations at Karlsruhe and Izaña). This indicates that the error budget and sensitivity characterization are realistic and correct.

5.5 Statistics of the agreement between FTIRs and IASI

Figure 12 gives a scatter plot of IASI vs. FTIR observations for the three different sites. The data refer to the δD at 2.5 km for Kiruna and Karlsruhe and at 5.5 km for Izaña, which are the altitudes for which the two instruments share the most sensitivity. The SD of the difference between IASI and FTIR for all the collocated measurements are 24, 35 and 55 ‰ for Kiruna, Karlsruhe and Izaña respectively which is in very good agreement with theoretical expected difference. The

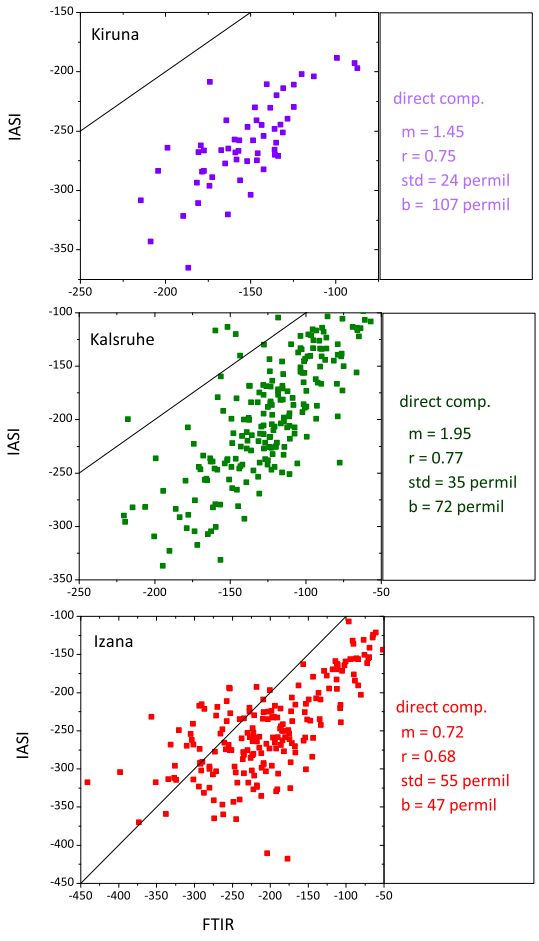

Figure 12. Scatter plot of IASI vs. FTIR δD from top to bottom for Kiruna (2.5 km), Karlsruhe (2.5 km) and Izaña (5.5 km). We give the slopes of the major axis regression curves (m), the Pearson correlation coefficient (r), the SD of the difference and the mean bias (b, FTIR-IASI).

correlation coefficients of 0.75, 0.77 and 0.68 indicate that δD retrieved from both instruments co-vary well together. The smaller correlation coefficient of 0.68 at Izaña compared to Kiruna and Karlsruhe is logical due to the larger difference expected at this site. The slope of the regression curves indicate that the amplitude of δD variations is more important for IASI than FTIR at Kiruna and Karlsruhe. But that the opposite prevails at Izaña.

For the three sites, IASI δD are biased low compared to FTIR. The mean bias values (FTIR-IASI) are 107, 72 and 47 ‰ for Kiruna, Karlsruhe and Izaña respectively. Since we are not considering exactly the same atmosphere in the different locations due to the impossibility of smoothing one retrieval with the averaging kernels of the other the values can not quantitatively be compared between them. Qualitatively, this bias appears to decrease with altitude and the value of 47 ‰ found at Izaña is close to what has been found in the recent absolute validation of ground-based FTIR by Schneider et al. (2014) where the authors found a high bias of the Izaña ground-based FTIR of +70 ‰ in the middle troposphere. In Wiegele et al. (2014), the authors used the same FTIR data to cross-validate the IASI/MUSICA product (retrieved at KIT/IMK-ASF) and found for all sites a consistently low bias. A direct comparison between the IASI/ULB product presented here and the IASI/MUSICA product would be interesting, but is out of the scope of this paper.

5.6 Variations of the log(q)–δD relation

To analyse the consistency of the humidity–δD relation between IASI and ground-based FTIR observations we follow a similar approach as that for comparison with TES. The idea is to see if IASI and ground-based FTIRs show coherent variations in the log(q)–δD space. We plot on Fig. 13 δD vs. humidity for the three different sites. δD (at 2.5 km for Kiruna and Karlsruhe and at 5.5 km for Izaña) are given in terms of relative variations to remove the biases discussed above. In the first three panels the different seasons are differentiated by colours. To better visualize spatial variations the comparison is also provided for all sites together but with colours to distinguish each (right panel). Since the different retrievals are not considering the same atmosphere this is a qualitative approach.

The extreme right panel of Fig. 13 shows that the three different sites exhibit very different distributions in the δD–log(q) space. The amplitudes of variations are very similar for IASI and the ground-based FTIR. The variability is the largest at Izaña with 400 ‰ between the minimum and maximum values, due to the fact that the retrieved value refers to the free troposphere (5.5 km) where the true variability is indeed expected to be large. The amplitude of variations is the lowest for Kiruna. At this site for which no winter collocated points were available, we observe a good agreement between the two distributions. The amplitudes of variations (for δD and H_2O) for both instruments are similar as well as the seasonal differences, although in the case of IASI the seasonal patterns appear to be more scattered. At Karlsruhe the general patterns agree best despite a steeper slope for IASI and shows well differentiated seasonal differences for both instruments. At Izaña IASI retrievals are more scattered than the FTIR ones owing to the larger observational error from IASI.

Overall Fig. 13 shows that IASI and the ground-based FTIR reproduce similar spatial and seasonal variations in humidity–δD relationships. We can safely conclude that the two instruments probe the same hydrological processes in the same way.

6 Conclusions

In this study we have cross-validated δD profiles retrieved from IASI spectra with profiles from TES and three ground-

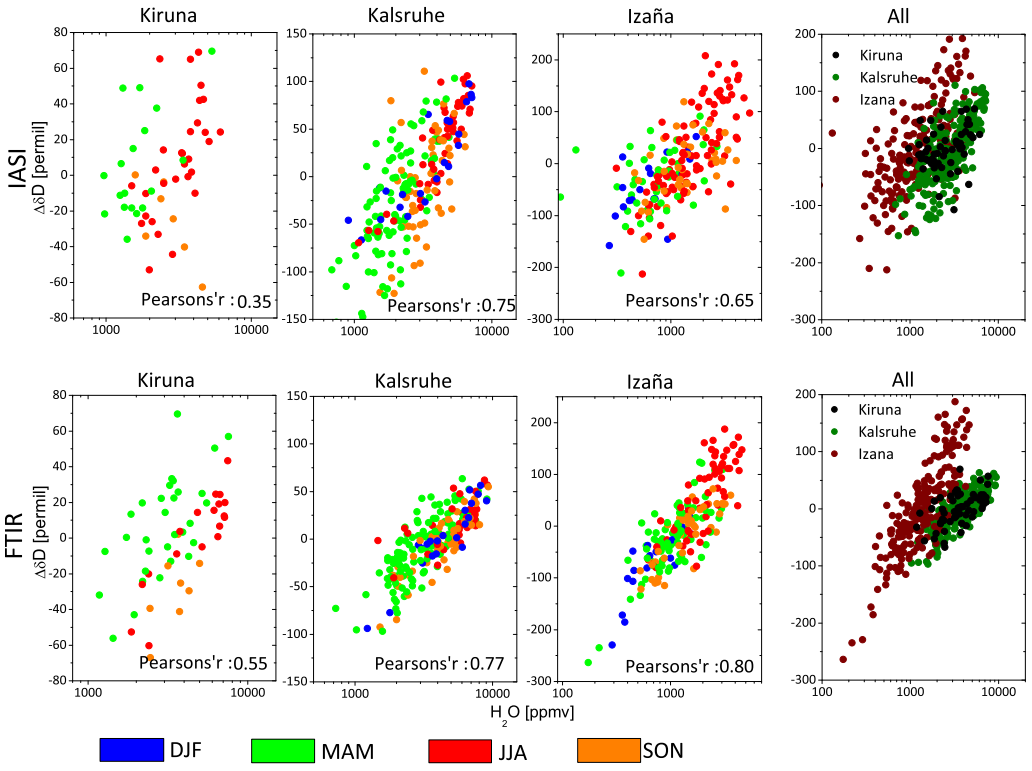

Figure 13. Distributions of IASI (top panels) and FTIR (bottom panels) observations in the $\log(q)$–δD space for the three different sites (from left to right: Kiruna, Karlsruhe and Izaña). The colours refer to seasons. Distributions for the three sites together are given on the right panel, with colours differentiating the sites: brown is for Izaña, green for Karlsruhe and yellow for Kiruna. δD values are presented in relative variations. Pearson correlation coefficients between δD and $\log(q)$ are also documented in the bottom of the plots.

based FTIRs. We provided a comprehensive and detailed estimation of error differences expected from the comparisons between the different instruments. Generally, we find that the total difference between TES and IASI, and between IASI and the ground-based FTIR is controlled by IASI observational error and by the smoothing error due to the differences in sensitivity of the instruments. In the comparison with the ground-based FTIRs, only a direct comparison was performed because it was not possible to simulate one retrieval with the averaging kernels of the other. The relevance of the different comparisons was analysed regarding the expected natural variability of δD at a global scale and also at regional scale. Except at Izaña, all the comparisons exhibit differences lower than expected natural variability at regional scales.

We have further verified the theoretical consistency of our error estimations and showed that they were consistent with the real differences in δD measured by the various instruments. This successful cross-validation of IASI has been performed at various locations from tropical to Arctic latitudes, above sea and land, giving us excellent confidence in the retrieved profiles from IASI at a global scale. Moreover, spatio-temporal variations of the humidity–δD relation were analysed and show coherent variations among the instruments, indicating that the latter were sensitive to the hydrological processes in the same way.

The cross-validation exercise performed here also allowed us to better characterize IASI retrievals. Above sea, we have shown that IASI retrievals exhibit large error in the lower and upper troposphere, exceeding the expected natural variability of δD. The retrieved profile is, on the contrary, exploitable in the free troposphere where the error is minimized. Above land, the large thermal contrast reduces the error in the lowest layers and allows one to retrieve profiles of δD down to the near surface with sufficient precision, as demonstrated with the comparison at Kiruna and Karlsruhe.

By analysing the empirical differences between IASI and the other sounders, we found a small bias with TES (−3 ‰ in the free troposphere) and an important bias with the FTIR (−47 ‰ in the free troposphere).

Finally, we have investigated the impact of IASI sampling in a model–instrument comparison and showed that the daily agreement between model and IASI was greatly improved when using all IASI observations available in a model cell. This suggests that model evaluation against observations could be optimized with IASI more than with other sounders (in the free troposphere).

Appendix A: Sensitivity change along the meridional gradient for IASI retrieval

Since IASI presents some sensitivity to surface we expect a change in sensitivity with decreasing surface temperature. This change is not visible on Fig. 4, in this appendix we further investigate this apparent contradiction. In Fig. A1, we used all available IASI data along the meridional gradient and average the degrees of freedom for H_2O and δD on latitude bins. For H_2O there is an increase in sensitivity with surface temperature and a small decrease is observed with high water vapour content. For δD we also observe a significant increase in DOFS with latitude but with a more significant drop off in sensitivity with high water vapour content. This could explain why IASI sensitivity is more constant with latitudinal variations than TES.

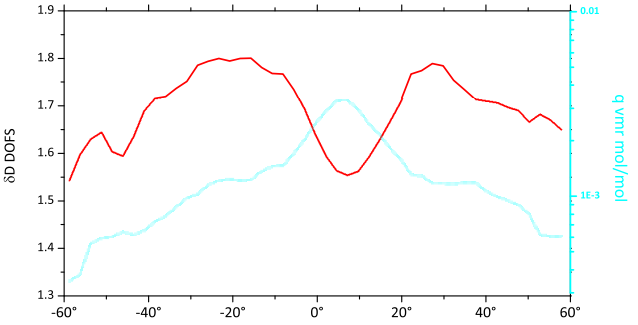

Figure A1. Variation of the degrees of freedom for IASI δD retrieval along the latitudinal gradient (red) and mixing ratio of water vapour at 4.5 km.

Acknowledgements. IASI has been developed and built under the responsibility of the "Centre National d'Etudes Spatiales" (CNES, France). It is flown onboard the MetOp satellites as part of the EUMETSAT Polar System. The IASI L1 data are received through the EUMETCast near real-time data distribution service. The research in Belgium was funded by the F.R.S.-FNRS, the Belgian State Federal Office for Scientific, Technical and Cultural Affairs (Prodex arrangement 4000111403 IASI.FLOW). L. Clarisse and P.-F. Coheur are respectively Research Associate (Chercheur Qualifié) and Senior Research Associate (Maître de Recherches) with F.R.S.-FNRS. C. Clerbaux is grateful to CNES for scientific collaboration and financial support. The ground-based FTIR retrievals have been performed in the framework of the project MUSICA, which is funded by the European Research Council under the European Community's Seventh Framework Programme (FP7/2007-2013)/ERC Grant agreement number 256961.

Edited by: L. Hoffmann

References

Allan, R. P., Ringer, M. A., and Slingo, A.: Evaluation of moisture in the Hadley Centre climate model using simulations of HIRS water-vapour channel radiances, Q. J. Roy. Meteorol. Soc., 129, 3371–3389, doi:10.1256/qj.02.217, 2003.

Bates, J. J. and Jackson, D. L.: A comparison of water vapor observations with AMIPI simulations, J. Geophys. Res., 102, 21837–21852, doi:10.1029/97JD01769, 1997.

Beer, R., Glavich, T. A., and Rider, D. M.: Tropospheric emission spectrometer for the Earth Observing System's Aura satellite, Appl. Optics, 40, 2356–2367, 2001.

Boesch, H., Deutscher, N. M., Warneke, T., Byckling, K., Cogan, A. J., Griffith, D. W. T., Notholt, J., Parker, R. J., and Wang, Z.: HDO / H_2O ratio retrievals from GOSAT, Atmos. Meas. Tech., 6, 599–612, doi:10.5194/amt-6-599-2013, 2013.

Brogniez, H. and Pierrehumbert, R. T.: Intercomparison of tropical tropospheric humidity in GCMs with AMSU-B water vapor data, Geophys. Res. Lett., 34, L17812, doi:10.1029/2006GL029118, 2007.

Calisesi, Y., Soebijanta, V. T., and van Oss, R.: Regridding of remote soundings: formulation and application to ozone profile comparison, J. Geophys. Res., 110, D23306, doi:10.1029/2005JD006122, 2005.

Ceccherini, S., Carli, B., Pascale, E., Prosperi, M., Raspollini, P., and Dinelli, B. M.: Comparison of measurements made with two different instruments of the same atmospheric vertical profile, Appl. Optics, 42, 6465–6473, doi:10.1364/AO.42.006465, 2003.

Cess, R. D., Potter, G. L., Blanchet, J. P., Boer, G. J., Del Genio, A. D., Déqué, M., Dymnikov, V., Galin, V., Gates, W. L., Ghan, S. J., Kiehl, J. T., Lacis, A. A., Le Treut, H., Li, Z.-X., Liang, X.-Z., McAvaney, B. J., Meleshko, V. P., Mitchell, J. F. B., Morcrette, J.-J., Randall, D. A., Rikus, L., Roeckner, E., Royer, J. F., Schlese, U., Sheinin, D. A., Slingo, A., Sokolov, A. P., Taylor, K. E., Washington, W. M., Wetherald, R. T., Yagai, I., and Zhang, M.-H.: Intercomparison and interpretation of climate feedback processes in 19 atmospheric general circulation models, J. Geophys. Res., 95, 16601–16615, doi:10.1029/JD095iD10p16601, 1990.

Clerbaux, C., Boynard, A., Clarisse, L., George, M., Hadji-Lazaro, J., Herbin, H., Hurtmans, D., Pommier, M., Razavi, A., Turquety, S., Wespes, C., and Coheur, P.-F.: Monitoring of atmospheric composition using the thermal infrared IASI/MetOp sounder, Atmos. Chem. Phys., 9, 6041–6054, doi:10.5194/acp-9-6041-2009, 2009.

Craig, H.: Isotopic variations in meteoric waters, Science, 133, 1702–1703, doi:10.1126/science.133.3465.1702, 1961.

de Forster, P. and Collins, M.: Quantifying the water vapour feedback associated with post-Pinatubo global cooling, Clim. Dynam., 23, 207–214, doi:10.1007/s00382-004-0431-z, 2004.

Draxler, R. R. and Hess, G. D.: An overview of the HYSPLIT4 modeling system for trajectories, dispersion and deposition, Aust. Meteorol. Mag., 47, 295–308, 1998.

Dufresne, J.-L. and Bony, S.: An assessment of the primary sources of spread of global warming estimates from coupled atmosphere? Ocean models, J. Climate, 21, 5135–5144, doi:10.1175/2008JCLI2239.1, 2008.

Frankenberg, C., Yoshimura, K., Warneke, T., Aben, I., Butz, A., Deutscher, N., Griffith, D., Hase, F., Notholt, J., Schneider, M., Schrijver, H., and Rockmann, T.: Dynamic processes governing lower-tropospheric HDO / H_2O ratios as observed from space and ground, Science, 325, 1374–1377, doi:10.1126/science.1173791, 2009.

Frankenberg, C., Wunch, D., Toon, G., Risi, C., Scheepmaker, R., Lee, J.-E., Wennberg, P., and Worden, J.: Water vapor isotopologue retrievals from high-resolution GOSAT shortwave infrared spectra, Atmos. Meas. Tech., 6, 263–274, doi:10.5194/amt-6-263-2013, 2013.

Galewsky, J., Strong, M., and Sharp, Z. D.: Measurements of water vapor D /H ratios from Mauna Kea, Hawaii, and implications for subtropical humidity dynamics, Geophys. Res. Lett., 34, L22808, doi:10.1029/2007GL031330, 2007.

Herman, R. L., Cherry, J. E., Young, J., Welker, J. M., Noone, D., Kulawik, S. S., and Worden, J.: Aircraft validation of Aura Tropospheric Emission Spectrometer retrievals of HDO / H_2O, Atmos. Meas. Tech., 7, 3127–3138, doi:10.5194/amt-7-3127-2014, 2014.

Hilton, F., Armante, R., August, T., Barnet, C., Bouchard, A., Camy-Peyret, C., Capelle, V., Clarisse, L., Clerbaux, C., Coheur, P.-F., Collard, A., Crevoisier, C., Dufour, G., Edwards, D., Faijan, F., Fourrié, N., Gambacorta, A., Goldberg, M., Guidard, V., Hurtmans, D., Illingworth, S., Jacquinet-Husson, N., Kerzenmacher, T., Klaes, D., Lavanant, L., Masiello, G., Matricardi, M., McNally, A., Newman, S., Pavelin, E., Payan, S., Péquignot, E., Peyridieu, S., Phulpin, T., Remedios, J., Schlüssel, P., Serio, C., Strow, L., Stubenrauch, C., Taylor, J., Tobin, D., Wolf, W., and Zhou, D.: Hyperspectral earth observation from IASI: five years of accomplishments, B. Am. Meteorol. Soc., 93, 347–370, doi:10.1175/BAMS-D-11-00027.1, 2012.

Hurtmans, D., Coheur, P.-F., Wespes, C., Clarisse, L., Scharf, O., Clerbaux, C., Hadji-Lazaro, J., George, M., and Turquety, S.: FORLI radiative transfer and retrieval code for IASI, J. Quant. Spectrosc. Ra., 113, 1391–1408, doi:10.1016/j.jqsrt.2012.02.036, 2012.

Lacour, J.-L., Risi, C., Clarisse, L., Bony, S., Hurtmans, D., Clerbaux, C., and Coheur, P.-F.: Mid-tropospheric δD observations from IASI/MetOp at high spatial and temporal resolu-

tion, Atmos. Chem. Phys., 12, 10817–10832, doi:10.5194/acp-12-10817-2012, 2012.

Noone, D.: Pairing measurements of the water vapor isotope ratio with humidity to deduce atmospheric moistening and dehydration in the tropical mid-troposphere, J. Climate, 25, 4476–4494, doi:10.1175/JCLI-D-11-00582.1, 2012.

Noone, D., Galewsky, J., Sharp, Z. D., Worden, J., Barnes, J., Baer, D., Bailey, A., Brown, D. P., Christensen, L., Crosson, E., Dong, F., Hurley, J. V., Johnson, L. R., Strong, M., Toohey, D., Van Pelt, A., and Wright, J. S.: Properties of air mass mixing and humidity in the subtropics from measurements of the D / H isotope ratio of water vapor at the Mauna Loa Observatory, J. Geophys. Res., 116, D22113, doi:10.1029/2011JD015773, 2011.

Pierce, D. W., Barnett, T. P., Fetzer, E. J., and Gleckler, P. J.: Three-dimensional tropospheric water vapor in coupled climate models compared with observations from the AIRS satellite system, Geophys. Res. Lett., 33, L21701, doi:10.1029/2006GL027060, 2006.

Pierrehumbert, R. T., Brogniez, H., and Roca, R.: On the Relative Humidity of the Earth's Atmosphere, Princeton University Press, Princeton, NJ, 2007.

Pommier, M., Lacour, J.-L., Risi, C., Bréon, F. M., Clerbaux, C., Coheur, P.-F., Gribanov, K., Hurtmans, D., Jouzel, J., and Zakharov, V.: Observation of tropospheric δD by IASI over western Siberia: comparison with a general circulation model, Atmos. Meas. Tech., 7, 1581–1595, doi:10.5194/amt-7-1581-2014, 2014.

Rayleigh, L.: On the distillation of binary mixtures, Philos. Mag., 4, 521–537, 1902.

Risi, C., Bony, S., and Vimeux, F.: Influence of convective processes on the isotopic composition of precipitation and water vapor in the tropics: 2. Physical interpretation of the amount effect, J. Geophys. Res., 113, D19306, doi:10.1029/2008JD009943, 2008.

Risi, C., Bony, S., Vimeux, F., and Jouzel, J.: Water-stable isotopes in the LMDZ4 general circulation model: model evaluation for present-day and past climates and applications to climatic interpretations of tropical isotopic records, J. Geophys. Res., 115, D12118, doi:10.1029/2009JD013255, 2010.

Risi, C., Noone, D., Worden, J., Frankenberg, C., Stiller, G., Kiefer, M., Funke, B., Walker, K., Bernath, P., Schneider, M., Bony, S., Lee, J., Brown, D., and Sturm, C.: Process-evaluation of tropospheric humidity simulated by general circulation models using water vapor isotopic observations: 2. Using isotopic diagnostics to understand the mid and upper tropospheric moist bias in the tropics and subtropics, J. Geophys. Res., 117, D05304, doi:10.1029/2011JD016623, 2012a.

Risi, C., Noone, D., Worden, J., Frankenberg, C., Stiller, G., Kiefer, M., Funke, B., Walker, K., Bernath, P., Schneider, M., Wunch, D., Sherlock, V., Deutscher, N., Griffith, D., Wennberg, P. O., Strong, K., Smale, D., Mahieu, E., Barthlott, S., Hase, F., Garcia, O., Notholt, J., Warneke, T., Toon, G., Sayres, D., Bony, S., Lee, J., Brown, D., Uemura, R., and Sturm, C.: Process-evaluation of tropospheric humidity simulated by general circulation models using water vapor isotopologues: 1. Comparison between models and observations, J. Geophys. Res., 117, D05303, doi:10.1029/2011JD016621, 2012b.

Rodgers, C. D.: Inverse Methods for Atmospheric Sounding: Theory and Practise, World Scientific, Singapore, 2000.

Rodgers, C. D. and Connor, B. J.: Intercomparison of remote sounding instruments, J. Geophys. Res., 108, 4116, doi:10.1029/2002JD002299, 2003.

Samuels-Crow, K. E., Galewsky, J., Hardy, D. R., Sharp, Z. D., Worden, J., and Braun, C.: Upwind convective influences on the isotopic composition of atmospheric water vapor over the tropical Andes, J. Geophys. Res.-Atmos., 119, 7051–7063, doi:10.1002/2014JD021487, 2014.

Schneider, M. and Hase, F.: Optimal estimation of tropospheric H_2O and δD with IASI/METOP, Atmos. Chem. Phys., 11, 11207–11220, doi:10.5194/acp-11-11207-2011, 2011.

Schneider, M., Hase, F., and Blumenstock, T.: Ground-based remote sensing of HDO / H_2O ratio profiles: introduction and validation of an innovative retrieval approach, Atmos. Chem. Phys., 6, 4705–4722, doi:10.5194/acp-6-4705-2006, 2006.

Schneider, M., Barthlott, S., Hase, F., González, Y., Yoshimura, K., García, O. E., Sepúlveda, E., Gomez-Pelaez, A., Gisi, M., Kohlhepp, R., Dohe, S., Blumenstock, T., Wiegele, A., Christner, E., Strong, K., Weaver, D., Palm, M., Deutscher, N. M., Warneke, T., Notholt, J., Lejeune, B., Demoulin, P., Jones, N., Griffith, D. W. T., Smale, D., and Robinson, J.: Ground-based remote sensing of tropospheric water vapour isotopologues within the project MUSICA, Atmos. Meas. Tech., 5, 3007–3027, doi:10.5194/amt-5-3007-2012, 2012.

Schneider, M., González, Y., Dyroff, C., Christner, E., Wiegele, A., Barthlott, S., García, O. E., Sepúlveda, E., Hase, F., Andrey, J., Blumenstock, T., Guirado, C., Ramos, R., and Rodríguez, S.: Empirical validation and proof of added value of MUSICA's tropospheric δD remote sensing products, Atmos. Meas. Tech., 8, 483–503, doi:10.5194/amt-8-483-2015, 2015.

Sherwood, S. C., Roca, R., Weckwerth, T. M., and Andronova, N. G.: Tropospheric water vapor, convection, and climate, Rev. Geophys., 48, RG2001, doi:10.1029/2009RG000301, 2010.

Sherwood, S. C., Bony, S., and Dufresne, J.-L.: Spread in model climate sensitivity traced to atmospheric convective mixing, Nature, 505, 37–42, doi:10.1038/nature12829, 2014.

Soden, B. J. and Bretherton, F. P.: Evaluation of water vapor distribution in general circulation models using satellite observations, J. Geophys. Res., 99, 1187–1210, doi:10.1029/93JD02912, 1994.

Soden, B. J. and Held, I. M.: An assessment of climate feedbacks in coupled ocean atmosphere models, J. Climate, 19, 3354–3360, doi:10.1175/JCLI3799.1, 2006.

Strong, M., Sharp, Z. D., and Gutzler, D. S.: Diagnosing moisture transport using D / H ratios of water vapor, Geophys. Res. Lett., 34, L03404, doi:10.1029/2006GL028307, 2007.

von Clarmann, T.: Validation of remotely sensed profiles of atmospheric state variables: strategies and terminology, Atmos. Chem. Phys., 6, 4311–4320, doi:10.5194/acp-6-4311-2006, 2006.

Wiegele, A., Schneider, M., Hase, F., Barthlott, S., García, O. E., Sepúlveda, E., González, Y., Blumenstock, T., Raffalski, U., Gisi, M., and Kohlhepp, R.: The MUSICA MetOp/IASI H_2O and δD products: characterisation and long-term comparison to NDACC/FTIR data, Atmos. Meas. Tech., 7, 2719–2732, doi:10.5194/amt-7-2719-2014, 2014.

Worden, J., Bowman, K., Noone, D., Beer, R., Clough, S., Eldering, A., Fisher, B., Goldman, A., Gunson, M., Herman, R., Kulawik, S. S., Lampel, M., Luo, M., Osterman, G., Rinsland, C.,

Rodgers, C., Sander, S., Shephard, M., and Worden, H.: Tropospheric Emission Spectrometer observations of the tropospheric HDO/H_2O ratio: estimation approach and characterization, J. Geophys. Res., 111, D16309, doi:10.1029/2005JD006606, 2006.

Worden, J., Noone, D., and Bowman, K.: Importance of rain evaporation and continental convection in the tropical water cycle, Nature, 445, 528–532, doi:10.1038/nature05508, 2007.

Worden, J., Noone, D., Galewsky, J., Bailey, A., Bowman, K., Brown, D., Hurley, J., Kulawik, S., Lee, J., and Strong, M.: Estimate of bias in Aura TES HDO/H_2O profiles from comparison of TES and in situ HDO/H_2O measurements at the Mauna Loa observatory, Atmos. Chem. Phys., 11, 4491–4503, doi:10.5194/acp-11-4491-2011, 2011.

Worden, J., Kulawik, S., Frankenberg, C., Payne, V., Bowman, K., Cady-Peirara, K., Wecht, K., Lee, J.-E., and Noone, D.: Profiles of CH_4, HDO, H_2O, and N_2O with improved lower tropospheric vertical resolution from Aura TES radiances, Atmos. Meas. Tech., 5, 397–411, doi:10.5194/amt-5-397-2012, 2012.

Yoshimura, K., Frankenberg, C., Lee, J., Kanamitsu, M., Worden, J., and Röckmann, T.: Comparison of an isotopic atmospheric general circulation model with new quasi-global satellite measurements of water vapor isotopologues, J. Geophys. Res., 116, D19118, doi:10.1029/2011JD016035, 2011.